Applied Physics A (2021) 127:92
https://doi.org/10.1007/s00339-020-04248-0

Applied Physics A
Materials Science & Processing

RAPID COMMUNICATIONS

2D-antimonene-based surface plasmon resonance sensor for improvement of sensitivity

Surjeet Raikwar[1] · D. K. Srivastava[1] · J. P. Saini[2] · Y. K. Prajapati[3]

Received: 11 November 2020 / Accepted: 23 December 2020 / Published online: 11 January 2021

Abstract

In this paper, a surface plasmon resonance sensor based on MXene and antimonene with an adhesive layer of TiO_2 is numerically analyzed, using the transfer matrix method (TMM). First, the Au thickness is optimized at 48 nm. Then, antimonene and MXene layers are optimized to achieve high sensitivity with minimum reflectance. The sensitivity of the proposed SPR biosensor without using the TiO_2 layer is 178.76°/RIU, which shows 6.34% sensitivity improvement than conventional SPR. The use of TiO_2 as an adhesive layer between prism and gold (Au) enhances the sensitivity up to 224.26°/RIU, which is 33.7 and 25.77% better than conventional and proposed SPR biosensor without using TiO_2, respectively. This is due to the attractive optical sensing properties of MXene (highly metallic conductivity) and antimonene (high carrier mobility, strong spin–orbit coupling, and stability). Here, antimonene is used as a biomolecular recognition element (BRE) layer, as it absorbs more biomolecules stably due to higher binding energies and larger surface area, even better than graphene.

Keywords Antimonene · MXene · Surface plasmon resonance sensor (SPR) · Limit of detection (LOD) · Sensitivity

1 Introduction

In recent years, 2D materials have played a vital role in the field of nanotechnology since the isolation of the first single-layer semimetal graphene from graphite by Novoselov et al. [1–6]. The widespread use of graphene in different areas related to biosensing, solar cells, electronic and photonic devices, etc. increases the curiosity of researchers in other 2D materials too [7–11]. In the context of biosensing, surface plasmon resonance (SPR) sensor has been largely explored for food safety, environmental monitoring, and disease diagnostics since the last 4 decades [12]. SPR sensor has witnessed widespread sensing applications among other optical sensors due to its fast, reliable, accurate, and cost-effective detection procedures [12]. SPR sensor detects the refractive index (RI) change on the binding of analyte or biomolecules. The conventional SPR sensors based on a single metal layer responsible for surface plasmons (SPs) generation and binding of analyte were unable to show enhanced performance. This research gap has given a scope to improve the SPR sensor performance by integrating different 2D materials atomic layer into conventional SPR devices [12]. The performance of 2D material-based SPR sensors mainly depends on their unique physical, chemical, electronic, and optical properties. A number of research groups reported the use of various new 2D materials like transition metal dichalcogenides (TMDs), black phosphorus, blue phosphorene, MXene ($Ti_3C_2T_x$), and antimonene, etc. in SPR sensor for gas, biochemical and biosensing, etc. [7, 13–19].

2D layered MXene ($Ti_3C_2T_x$) has shown their capabilities of hydrophilic surface terminations with a larger area, chemically stable, higher binding energies, and high metallic

✉ Y. K. Prajapati
yogendrapra@mnnit.ac.in

Surjeet Raikwar
surjeet1255@gmail.com

D. K. Srivastava
dks1_biet@rediffmail.com

J. P. Saini
jps@nsut.ac.in

[1] Department of Electronics and Communication Engineering, Bundelkhand Institute of Engineering and Technology (BIET), Jhansi, U.P. 284128, India

[2] Department of Electronics and Communication Engineering, Netaji Subhas University of Technology (NSUT), New Delhi 110078, India

[3] Department of Electronics and Communication Engineering, Motilal Nehru National Institute of Technology Allahabad, Prayagraj, U.P. 211004, India

conductivity to improve SPR sensor performance [17]. 2D layered MXene ($Ti_3C_2T_x$) is prepared by extracting Al from its corresponding MAX phase (Ti_3AlC_2) using hydrofluoric (HF) acid and then obtaining nanosheets using liquid exfoliation method [17]. Recently, Chen et al. proposed RI detection-based Au-$Ti_3C_2T_x$ fiber optic SPR sensor for sensing of biochemical molecules [17]. A. Srivastava et al. presented an Au/$Ti_3C_2T_x$/WS_2/BP-based SPR sensor to enhance the sensitivity up to 190.2°/RIU [18].

The different attachment strategy for binding of biomolecules with the interacting layer plays a very important role for precise and reliable sensing. In this context, graphene is highly advantageous for increased adsorption of carbon-based biomolecules with π bonds of graphene [19]. Recently, a new 2D material antimonene is exfoliated from bulk antimony (Sb) which has sp^2-bonded honeycomb lattice structure similar to graphene [6]. It has shown tremendous stability, hydrophilicity, and higher adsorption energies even greater than graphene for the attachments of ssDNA [7]. On comparing useful sensing properties of antimonene with other 2D nanomaterials, it has been observed that graphene suffers from the absence of a bandgap, and transition metal dichalcogenides (TMD) exhibits preferable band gaps, but it remains very challenging to achieve high carrier mobility and Black phosphorus (BP) shows both high carrier mobility (1000 cm^2/V/s) and tunable direct bandgap, but suffers from poor stability, especially upon exposure to light, water and oxygen [20]. The development of novel 2D material antimonene possesses high carrier mobility, suitable band gap above 2 eV (0–2.28 eV), and good stability that are suitable for sensing application [21]. On comparing it with black phosphorous, the most significant advantage of antimonene comes from its high stability and antioxidant capacity, which plays a critical role in practical sensing applications [21]. Although, the practical applications are somehow hindered due to the difficulty in preparing high-quality large-size 2D antimonene, due to its short layer distance and strong binding energy. To obtain antimonene successfully, various exfoliation techniques are available, but most of the reported methods suffer from some shortcomings, such as low yield or excessive time consumption [20]. However, recently, Tianyu Xue et al. proposed an Au nanorod-antimonene SPR sensor for detection of miRNA-21 and miRNA-15 [7]. This group performed first-principles energetic calculations (DFT-based) and found that antimonene has a stronger interaction with ssDNA than the graphene because of more delocalized 5s/5p orbitals in antimonene. Finally, this group verified experimentally that the detection limit is 10 aM, and the highest sensitivity achieved was 171°/RIU for four layers of antimonene [7]. Recently, Maneesh et al. proposed an SPR biosensor based on hetero-structure of BlueP/MoS_2 and antimonene for sensitivity enhancement up to 198.4°/RIU [8].

Not only 2D nanomaterials, but the carbon nanotube (CNT), MoO_3-based portable gas sensor, and Mxene-based screen-printed electrode for a direct and continuous multicomponent analysis of whole blood were also investigated in the literature [22–24]. The use of a high refractive index thin layer of oxides like silicon dioxide (SiO_2), titanium dioxide (TiO_2), and zinc oxide (ZnO) in combination with plasmonic metal to form a bimetallic layer generates a strong SPR effect [25–29]. This bimetallic structure enhances the sensitivity by generating more SPs at the interface of the metal/glass substrate [28]. Maurya et al. used composite layers of TiO_2–SiO_2 as an adhesion layer between prism with a hybrid structure of graphene-MoS_2 to improve the sensitivity of the SPR sensor [26]. However, these oxides do not possess the excellent adsorption properties for attachment of biomolecules (Fig. 1).

The proposed SPR sensor model consists of BK7 Prism–TiO_2–Au–MXene–antimonene based on Kretschmann configuration to enhance the sensitivity. Sections 2 and 3 present the proposed sensor modeling and the analysis of the results demonstrating the sensor's ability, respectively. Finally, Sect. 4 presents the concluding remarks for the proposed work.

2 Design consideration and numerical analysis

2.1 SPR structural overview

The present sensor comprising layers are BK7 prism, TiO_2, Au, MXene ($Ti_3C_2T_x$), and antimonene. The thicknesses and refractive indices of all layers used for the proposed design are mentioned in Table 1. The adhesiveness of silica-based prism is low with a gold layer that degrades the sensitivity of biosensor. The use of TiO_2 as an adherence layer over the glass substrate can overcome this issue, like its high and

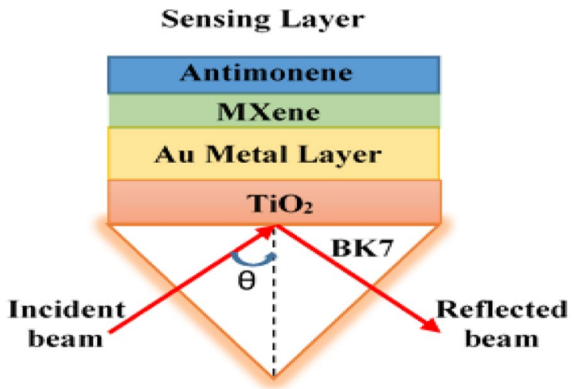

Fig.1 Structure of proposed SPR

Table 1 Optimized thickness and RI of different layers

Layer	Material used	Refractive index (RI) at 633 nm		Optimized thickness (nm)
		Real (n)	Imag. (ik)	
1	BK7 prism [15]	1.5151	–	
2	TiO_2 [27]	2.5837	–	0–4
3	Metal (Au) [18]	0.19683	3.0905	45
4	MXene [18]	2.38	1.33	0.993
5	Antimonene [8]	2.1	0.45	3
6	Sensing layer	1.330–1.335	–	–

Table 2 SPR sensor structures and layer arrangement

Structure	Layer arrangement
1	Prism/Au/sensing medium
2	Prism/Au/antimonene/sensing medium
3	Prism/Au/MXene/antimonene/sensing medium
4 proposed	Prism/TiO_2/Au/MXene/antimonene/sensing medium

purely real RI enhances the plasmonic effect to trap the light effectively [27, 28]. Due to trapping of light, more SPs are formed, and a large swing in resonance angle is observed, which increases the SPR sensitivity [19]. The plasmonic active metal layer, gold (Au) issued over TiO_2 for SPs generation [25]. Thereafter, 2D nanomaterial MXene ($Ti_3C_2T_x$) is used in direct contact over plasmonic metal Au, to significantly improve sensor sensitivity and signal-to-noise ratio (SNR) [29]. Topmost layer antimonene issued as BRE layer for attachment of biomolecules [30]. An aqueous solution containing biomolecules to be sensed is used as a sensing medium with RI, $n_s = 1.33$. The biomolecules' attachment on antimonene surface leads to a shift in sensing medium RI to a new value, i.e., $n_s = 1.33 + \Delta n_s$. To achieve the resonance phenomenon, a 633 nm wavelength of p-polarized incident light is coupled to surface plasmon wave (SPW) using BK7 prism. Using attenuated total reflection (ATR), resonance condition is achieved after the proper matching of wave vector of incident light with SPW. The resonance angle at which SPR condition attained is very sensitive to RI shift of sensing layer of the biomolecule, which disturbs the resonance condition. It may be regained by changing the incident angle. The different sensor structures used for comparison with the proposed work are given in Table 2.

2.2 SPR sensor mathematical formulation

For numerical simulations, transfer matrix method (TMM) is used for the calculation of reflectance [8]. The tangential components of electromagnetic fields are given as:

$$\frac{B_1}{C_1} = A_2A_3A_4 \ldots A_{N-1}\begin{bmatrix} B_{N-1} \\ C_{N-1} \end{bmatrix} = A\begin{bmatrix} B_{N-1} \\ C_{N-1} \end{bmatrix}, \tag{1}$$

where, B_1, B_{N-1}, and C_1, C_{N-1} are the tangential components of electric and magnetic fields, respectively, at the boundary of 1stand Nth layer. For combined structure, the characteristic matrix A is defined as:

$$A = \prod_{k=2}^{N-1} A_k = \begin{bmatrix} A_{11} & A_{12} \\ A_{21} & A_{22} \end{bmatrix}. \tag{2}$$

Here:

$$\mathrm{A}_k = \begin{bmatrix} \cos\beta_k & -i\sin\left(\beta_k/q_k\right) \\ -iq_k\sin\beta_k & \cos\beta_k \end{bmatrix}, \tag{3}$$

$$q_k = \left(\frac{\mu_k}{\varepsilon_k}\right)^{1/2}\cos\theta = \left(\frac{\varepsilon_k - n_1^2\sin^2\theta_1}{\varepsilon_k}\right)^{1/2}, \tag{4}$$

$$\beta_k = \frac{2\Pi}{\lambda}\left(\varepsilon_k - n_1^2\sin^2\theta_1\right)^{1/2}. \tag{5}$$

In Eqs. (4) and (5), β_k and q_k represent optical admittance and phase factor of the kth layer, respectively. Here, n_1, θ_1, λ, ε_k, and μ_k denote prism RI, incident angle, and wavelength of the incident light, dielectric constant, and permeability of the kth layer, respectively.

Using some forward steps, amplitude of reflection coefficient (r) and reflectivity (R) for p-polarized light are calculated by:

$$R = |r|^2 = \frac{\left(A_{11} + A_{12}q_N\right)q_1 - \left(A_{21} + A_{22}q_N\right)}{\left(A_{11} + A_{12}q_N\right)q_1 + \left(A_{21} + A_{22}q_N\right)}. \tag{6}$$

2.3 SPR sensor performance formulation

2.3.1 Sensitivity (S)

Sensitivity (S) is a ratio of resonance angle shift (θ_{spr}) to minute change of sensing layer RI, and it is expressed as:

$$S = \frac{\delta\theta_{spr}}{\delta n_s} \quad \text{(unit: °/RIU)}. \tag{7}$$

2.3.2 Detection accuracy (DA) or signal-to-noise ratio (SNR)

Detection accuracy (DA) or Signal-to-Noise ratio (SNR) is inversely related to full width at half maximum FWHM and FWHM measures the angular width of SPR curve:

$$\mathrm{DA} = \frac{1}{\mathrm{FWHM}} \quad (\text{unit: } /\circ). \tag{8}$$

2.3.3 Figure of merit (FoM)

Figure of merit (FoM) is the ratio of sensitivity to FWHM; its unit is /RIU:

$$\mathrm{FoM} = \frac{\delta\theta_{\mathrm{spr}}}{\delta n_{\mathrm{s}} \times \mathrm{FWHM}} \quad (\text{unit: /RIU}). \tag{9}$$

2.3.4 Limit of detection (LOD)

Limit of detection (LOD) measures the concentration quantitatively of biomolecules/analyte in sensing medium and defined as:

$$\mathrm{LOD} = \frac{\delta n_{\mathrm{s}}}{\delta\theta_{\mathrm{res}}} \times 0.001^{\circ}. \tag{10}$$

LOD is calculated for very minute change in sensing medium; here, we take shift 0.001°.

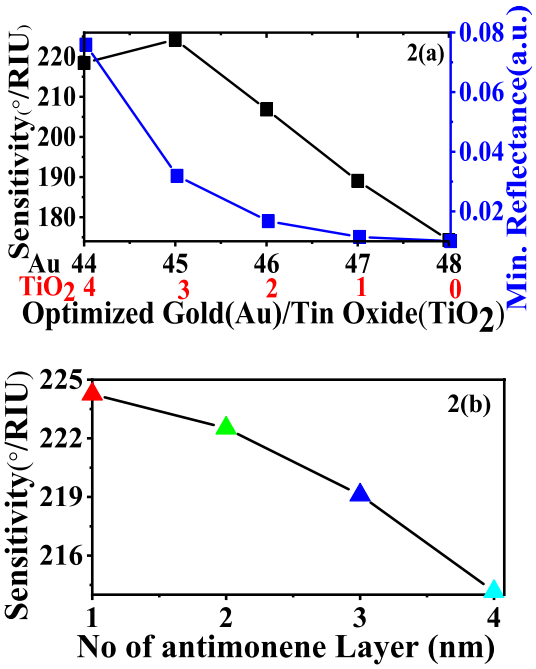

Fig. 2 **a** Thickness optimization of TiO_2/gold layer. **b** Layer optimization of antimonene

3 Results and discussion

The thicknesses of gold (Au) and TiO_2were optimized for maximum sensitivity and minimum reflection intensity (R_{min}). Figure 2a shows that the sensitivity and R_{min} with respect to different thicknesses of Au and TiO_2. At 45 and 3 nm thicknesses of Au and TiO_2, respectively, the maximum sensitivity reaches 224.26°/RIU at $R_{\mathrm{min}} = 0.0241$ a.u. The minimum value of R_{min} near zero shows the minimum energy loss to transfer the energy from incident light to SPs.

After the thickness optimization of SPR active metal Au and dielectric layer TiO_2, we optimized the antimonene layer. Figure 2b shows the sensitivity with respect to a number of antimonene layers. It is observed from Fig. 2b that the monolayer antimonene gives maximum sensitivity and it decreases for further increment in antimonene layers. Therefore, for the proposed SPR structure, we considered the monolayer of antimonene.

The most suitable SPR active metal is gold (Au) due to its chemical stability and oxidation resistance [27]. The SPR characteristic curve of gold (Au)-based conventional SPR for $\Delta n_{\mathrm{s}} = 0.005$ is shown in Fig. 3a. The conventional SPR structure shows that the variation in resonance angle, R_{min}, and corresponding sensitivity are 0.8933°, 0.0012 a.u., and 167.98°/RIU, respectively. On employing 2D nanomaterial over the SPR active metal, the sensitivity increases [27, 28]. In this proposed work, 2D nanomaterials MXene and antimonene are used to enhance SPR biosensor's sensitivity by utilizing their unique sensing properties.

Figure 3b–d shows the SPR curves for sensor structures 2–4 at sensing medium RI variation from 1.330 to 1.335, and their SPR structures are shown as inset diagrams. The SPR curves for structure 2 (Au/antimonene) are shown in Fig. 3b. The variation in resonance angle ($\delta\theta$) obtained is 0.8681° at $R_{\mathrm{min}} = 0.0238$ a.u. and their corresponding sensitivity obtained is 173.62°/RIU. It is clearly seen that the resonance angle shift and sensitivity are higher than structure 1, when employing the antimonene over the Au. This is because biomolecules bind on antimonene with higher adsorption energies [8]. The SPR curve for structure 3 (Au/MXene/antimonene) is shown in Fig. 3c. The resonance angle shift ($\delta\theta$), R_{min}, obtained from Fig. 3c are 0.8938°, 0.0425 a.u., and the corresponding sensitivity calculated is 178.76°/RIU. Here, the use of MXene layer increases the transfer of charge carrier from antimonene to the metal–dielectric interface [18]. The SPR curve for structure 4 (TiO_2/Au/MXene/antimonene) is shown in Fig. 3d. A thin layer of titanium oxide (TiO_2) introduced in proposed SPR assists in adhering the Au layer to the BK7 prism. The variation in resonance angle ($\delta\theta$), R_{min}, obtained from Fig. 3d are 1.1213°, 0.0241 a.u., respectively, and corresponding sensitivity calculated is 224.26°/RIU. The sensitivity of proposed structure is much larger than previous structures owing to high pure RI of TiO_2 layer that provide large swing in resonance angle, and resulting in high sensitivity. Figure 4a shows

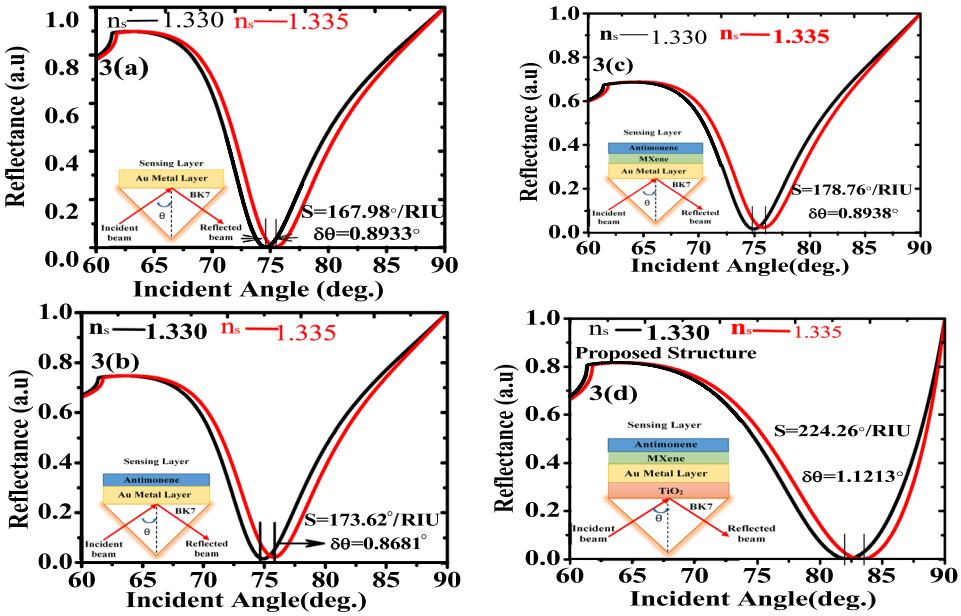

Fig. 3 SPR curves: **a** structure 1, **b** structure 2, **c** structure 3, and **d** structure 4 (proposed SPR sensor)

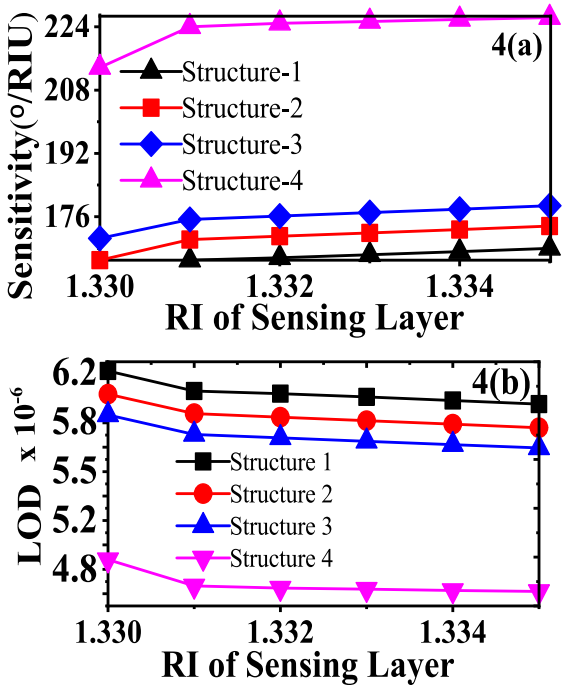

Fig. 4 Comparison of **a** sensitivity and **b** LOD vs. sensing layer RI for structure 1–4

the variation in sensitivity for all proposed structures with respect to variation in RI of sensing medium from 1.330 to 1.335 RIU. The sensitivity of structures 1, 2, 3, and 4 varies from 160.66°/RIU to 167.98°/RIU, 165.7°/RIU to 173.62°/RIU, 170.52°/RIU to 178.76°/RIU, and 213.72°/RIU to 224.26°/RIU, respectively, with respect to variation in RI of sensing medium. The use of TiO_2, MXene and antimonene in the proposed design provides the highest sensitivity owing to their unique optical properties useful for sensing applications. TiO_2 assists in reducing the adhesion problem of Au with silicate glass prism, and it is also helpful for exciting the SPR by efficiently contacting the prism-guided mode to the SPP mode. The MXene acts as a fast charge transmission bridge between Au and antimonene due to narrow bandgap and fast electron transfer ability. Antimonene has higher binding energies and a larger surface area that provides a stable and hydrophilic environment for attachment of biomolecules to increase the sensitivity of the sensor.

Next, in sequence, the LOD is calculated from Eq. (10) for all SPR structures proposed in Table 1. Figure 4b shows the variation of LOD with respect to variation in RI of sensing medium from 1.330 to 1.335 RIU. The LOD of sensor structure 1, 2, 3, and 4 varies from 6.22×10^{-6} to 5.95×10^{-6}, 6.03×10^{-6} to 5.75×10^{-6}, 5.86×10^{-6} to 5.59×10^{-6}, and 4.67×10^{-6} to 4.45×10^{-6}, respectively, with respect to variation in RI of sensing medium from 1.330 to 1.335 RIU. The lowest LOD is obtained for proposed structure 4 due to the highest variation in resonance angle. Now, in Fig. 5, the sensitivity, DA, and figure of merit are plotted with respect to RI of sensing medium at an optimized thickness of Au, TiO_2, and antimonene layers. The sensitivity, DA, and FoM are plotted using black, blue, and red colors.

The maximum sensitivity attained for the proposed SPR sensor is 224.26°/RIU, at $R_{min}=0.0241$ a.u. The DA and FoM calculated from Eqs. (8) and (9) are 0.084985/° and 19.05871/RIU. Here, LOD for the proposed structure is also calculated; for the proposed sensor, LOD is 4.41852×10^{-6}, which is lower than the conventional sensor and shown in Fig. 4b.

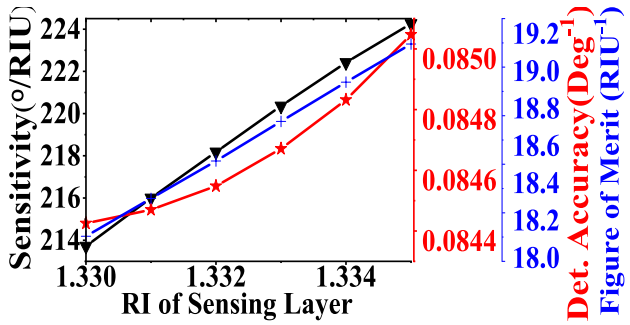

Fig. 5 The variation of sensitivity, detection accuracy, and FoM vs. sensing layer RI for the proposed sensor

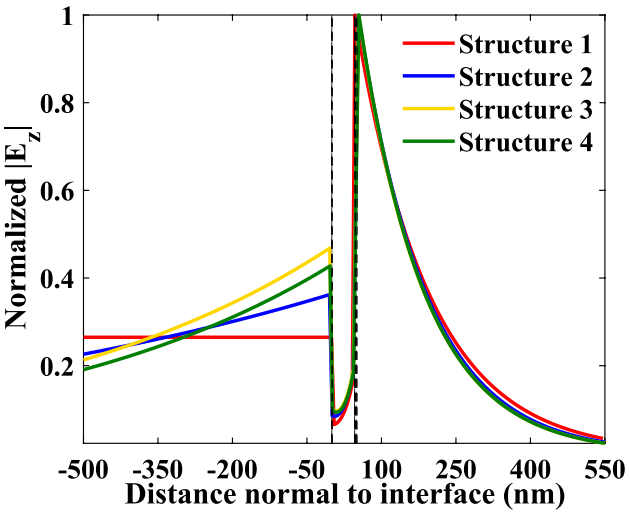

Fig. 6 Normalized transfer magnetic electric filed for considered structures

The distribution of the normalized electric field in different layers is shown in Fig. 6. In each layer, an electric field is normalized with the maximum electric field. An increment in the thickness of antimonene reduced the electric field intensity in the layer, so plasmons get damped, i.e., the electric field decreases exponentially in the sensing layer. The penetration depth is a function of wavelength, which signifies the deep penetration of light into the sensing layer material. Penetration depth is calculated as a maximum electric field at the sensing layer to $1/e$ of the maximum electric field. The high value shows high interaction with bio-species [18].

Table 3 shows the output of the SPR curves with pure water and after adsorption of biomolecules of different structures' configuration. The change in resonance angle, minimum reflectivity, FWHM, sensitivity, detection accuracy, the figure of merit, and limit of detection calculated for the structures 1–structure 4 as per Table 2 are shown in Table 3. The proposed structure (structure 4) depicts the highest sensitivity (224.26°/RIU), FOM (19.058/RIU) with the lowest LOD of 4.41 µM, respectively. Table 4 shows the comparison of the performance of proposed SPR with biosensors developed in the literature to detect biomolecules in terms of sensitivity, detection accuracy, the figure of merit, and limit of detection. The proposed biosensor shows the smallest LOD and highest sensitivity compared to other developed biosensors.

Table 3 Comparative study of sensitivity, detection accuracy, FOM, and LOD for proposed work

Configuration	$\Delta\theta_{spr}$	R_{min}	FWHM	S (°/RIU) at $\delta_n = 0.005$	DA (/°)	FOM (/RIU)	LOD ($\times 10^{-6}$)
Structure 1	0.8399	0.0012	9.3856	167.98	0.106546	17.89763	5.95309
Structure 2	0.8824	0.0238	9.7976	176.48	0.02066	18.01257	5.75971
Structure 3	0.8932	0.0425	10.3654	178.64	0.096475	17.23426	5.59409
Structure 4 (proposed)	1.1213	0.0241	12.0258	224.26	0.084985	19.05871	4.41852

Table 4 Comparative study of sensitivity with relevant research work

S. no.	References	Structure used	S (°/RIU)	DA (/°)	FOM (/RIU)	LOD ($\times 10^{-6}$)
1	Xue et al. [7]	Prism–Au–antimonene–sensing layer	171	–	–	–
2	Maneesh et al. [8]	Prism (BK7)–Au–antimonene–sensing layer	181.9	0.145	26.400	–
3	Gan et al. [31]	Prism (BK7)–Ag–franckeite–sensing layer	188	–	37.6	–
4	Wu et al. [19]	Prism (BK7)–air–MoS_2–Al–MoS_2–graphene–sensing layer	190.83	–	–	–
5	Proposed (structure 4)	Prism–TiO_2–Au–MXene–antimonene–sensing layer	224.26	0.084985	19.05871	4.41852

4 Conclusions

The antimonene-based SPR biosensor is developed to detect the biomolecules. The angle interrogation method is used for numerical analysis of the proposed biosensor. It is observed that only antimonene layer (structure II) enhanced the 5% sensitivity over conventional SPR biosensors. The hybrid structure of MXene and antimonene enhanced the sensitivity to 178.64°/RIU, owing to their admirable optical sensing properties. In a proposed biosensor, the adhesive layer of TiO_2 brought the sensitivity to 224.26°/RIU, which is 33.7% high compared to conventional SPR. A suitable range of the refractive index is used for analyzing the performance of the proposed work. The proposed work opens the door for new opportunities in the field of biosensing applications.

Acknowledgements This work is supported by Dr. Abdul Kalam Technical University, Lucknow (India) under the Ph.D. Scheme, Homi Bhabha Teaching Assistant Research Fellowship. And this work is also partially supported by Science and Engineering Research Board (SERB), India (Project Grant: CRG/2019/002636).

References

1. K.S. Novoselov, A.K. Geim, S.V. Morozov, D. Jiang, Y. Zhang, S.V. Dubonos, I.V. Grigorieva, A.A. Firsov, Electric field effect in atomically thin carbon films. Science **306**(5696), 666–669 (2004)
2. S. Guo, Y. Zhang, Y. Ge, S. Zhang, H. Zeng, H. Zhang, 2D V–V binary materials: status and challenges. Adv. Mater. **31**(39), 1902352 (2019)
3. J. Pei, J. Yang, T. Yildirim, H. Zhang, Y. Lu, Many body complexes in 2D semiconductors. Adv. Mater. **31**(2), 1706945 (2019)
4. X. Jiang, A.V. Kuklin, A. Baev, Y. Ge, H. Ågren, H. Zhang, P.N. Prasad, Two-dimensional MXenes: from morphological to optical, electric, and magnetic properties and applications. Phys. Rep. **848**, 1–58 (2020)
5. J. He, L. Tao, H. Zhang, B. Zhou, J. Li, Emerging 2D materials beyond graphene for ultrashort pulse generation in fiber lasers. Nanoscale **11**, 2577–2593 (2019)
6. P. Ares, F. Galindo et al., Mechanical isolation of highly stable antimonene under ambient condition. Adv. Mater. **28**(30), 6332–6336 (2016)
7. T. Xue, W. Liang, Y. Li, Y. Sun, Y. Xiang, Y. Zhang, Z. Dai, Y. Duo, L. Wu, K. Qi, B.N. Shivananju, Ultrasensitive detection of miRNA with an antimonene-based surface plasmon resonance sensor. Nat. Commun. **10**(1), 1–9 (2019)
8. M.K. Singh, S. Pal, Y.K. Prajapati, J.P. Saini, Sensitivity improvement of surface plasmon resonance sensor on using BlueP/MoS_2 heterostructure and antimonene. IEEE Sens. Lett. **4**(7), 1–4 (2020)
9. K. Wu, H. Ma, Y. Gao, W. Hu, J. Yang, Highly-efficient heterojunction solar cells based on two-dimensional tellurene and transition metal dichalcogenides. J. Mater. Chem. A **7**(13), 7430–7436 (2019)
10. R. Worsley, L. Pimpolari, D. McManus, N. Ge, R. Ionescu, J.A. Wittkopf, A. Alieva, G. Basso, M. Macucci, G. Iannaccone, K.S. Novoselov, All-2D material inkjet-printed capacitors: toward fully printed integrated circuits. ACS Nano **13**(1), 54–60 (2018)
11. X. Wang, Y. Cui, T. Li, M. Lei, J. Li, Z. Wei, Recent advances in the functional 2D photonic and optoelectronic devices. Adv. Opt. Mater. **7**(3), 1801274 (2019)
12. J. Homola, S.S. Yee, G. Gauglitz, Surface plasmon resonance sensors. Sens. Actuators B Chem. **54**(1–2), 3–15 (1999)
13. S. Pal, N. Pal, Y.K. Prajapati, J.P. Saini, Sensitivity analysis of surface plasmon resonance biosensor based on heterostructure of 2D BlueP/MoS_2 and MXene: layered advanced materials and their allied applications, in *Layered 2D advanced materials and their allied applications*. ed. by I. Inamuddin, R. Boddula (Scrivener Publication, Wiley, New York, 2020), pp. 103–125
14. Q. Wu, N. Li, Y. Wang, Y. Xu, S. Wei, J. Wu, G. Jia, X. Fang, F. Chen, X. Cui, A 2D transition metal carbide MXene-based SPR biosensor for ultrasensitive carcinoembryonic antigen detection. Biosens. Bioelectron. **144**, 111697 (2019)
15. T. Srivastava, R. Jha, Black phosphorus: a new platform for gaseous sensing based on surface plasmon resonance. IEEE Photon. Technol. Lett. **30**(4), 319–322 (2018)
16. S. Pal, A. Verma, J.P. Saini, Y.K. Prajapati, Sensitivity enhancement using silicon-black phosphorus-TDMC coated surface plasmon resonance biosensor. IET Optoelectron. **13**(4), 196–201 (2019)
17. Y. Chen, Y. Ge et al., Refractive index sensors based on $Ti_3C_2T_x$ MXene fibers. ACS Appl. Nano Mater. **3**(1), 303–311 (2020)
18. A. Srivastava, A. Verma, R. Das, Y.K. Prajapati, A theoretical approach to improve the performance of SPR biosensor using MXene and black phosphorus. Optik **203**, 163430 (2020)
19. L. Wu, H.S. Chu, W.S. Koh, E.P. Li, Highly sensitive graphene biosensors based on surface plasmon resonance. Opt. Express **18**(14), 14395–14400 (2010)
20. Q. Xiao et al., Antimonene-based flexible photodetector. Nanoscale Horiz. **5**, 124 (2020)
21. Y. Song et al., Few-layer antimonene decorated microfiber: ultra-short pulse generation and all-optical thresholding with enhanced long term stability. 2D Mater. **4**(4), 045010 (2017)
22. P. Wan, X. Wen, C. Sun, B.K. Chandran, H. Zhang, X. Sun, X. Chen, Flexible Transparent films based on nanocomposite networks of polyaniline and carbon nanotubes for high-performance gas sensing. Small **1**(40), 5409–5415 (2015)
23. S. Yang, Y. Liu, W. Chen, W. Jin, J. Zhou, H. Zhang, G.S. Zakharova, High sensitivity and good selectivity of ultralong MoO_3 nanobelts for trimethylamine gas. Sens. Actuators B Chem. **226**, 478–485 (2016)
24. J. Liu, X. Jiang, R. Zhang, Y. Zhang, L. Wu, W. Lu, J. Li, Y. Li, H. Zhang, MXene enabled electrochemical microfluidic biosensor: applications toward multicomponent continuous monitoring in whole blood. Adv. Funct. Mater. **29**(6), p1807326 (2019)
25. J. Xu, X. Xiao, A.L. Stepanov, F. Ren, W. Wu, G. Cai, S. Zhang, Z. Dai, F. Mei, C. Jiang, Efficiency enhancements in Ag nanoparticles-SiO_2–TiO_2 sandwiched structure via plasmonic effect-enhanced light capturing. Nanoscale Res. Lett. **8**(1), 1–5 (2013)
26. J.B. Maurya, Y.K. Prajapati, V. Singh, J.P. Saini, Sensitivity enhancement of surface plasmon resonance sensor based on graphene–MoS_2 hybrid structure with TiO_2–SiO_2 composite layer. Appl. Phys. A **121**(2), 525–533 (2015)
27. S. Singh, Y.K. Prajapati, TiO_2/gold-graphene hybrid solid core SPR based PCF RI sensor for sensitivity enhancement. Optik **1**(224), 165525 (2020)
28. M.A. Mahfuz, M. Hossain, E. Haque, N.H. Hai, Y. Namihira, F. Ahmed, A bimetallic-coated, low propagation loss, photonic crystal fiber based plasmonic refractive index sensor. Sensors **19**(17), 3794 (2019)
29. S. Pal, Y.K. Prajapati, J.P. Saini, Influence of graphene's chemical potential on SPR biosensor using ZnO for DNA hybridization. Opt. Rev. **27**(1), 57–64 (2020)

30. S. Pal, A. Verma, Y.K. Prajapati, Influence of black phosphorous on performance of surface plasmon resonance biosensor. Opt. Quant. Electron. **49**(12), 403 (2017)
31. S. Gan, Y. Zhao, X. Dai, Y. Xiang, Sensitivity enhancement of surface plasmon resonance sensors with 2D franckeite nanosheets. Results Phys. **13**, 102320 (2019)